Shock Waves (2003) 13: 25–32
Digital Object Identifier (DOI) 10.1007/s00193-003-0195-0

Shock Waves

A note on numerical simulation of vortical structures in shock diffraction

M. Sun, K. Takayama

Institute of Fluid Science, Tohoku University, Sendai 980-8577, Japan

Received 28 March 2003 / Accepted 6 May 2003
Published online 11 June 2003 – © Springer-Verlag 2003
Communicated by H. Grönig

Abstract. In numerical simulation of the Euler equations, the slipstream or shear layer that appears behind a diffracted shock wave may develop small discrete vortices using fine computational meshes. Similar phenomena were also observed in the simulation of a Mach reflection that is accompanied by a shear layer. However, these small vortices have never been observed in any shock-tube experiment, although the wave pattern and the shape of the main vortex agree very well with visualization results. Numerical solutions obtained with coarse grids may agree better with experimental photos than those with very fine grids because of the pollution of the small vortices. This note tries to investigate the effect of viscosity on the small vortices by comparing the solutions of the laminar Navier-Stokes equations and the $k-\epsilon$ turbulence model. It is found that the small vortices are still observed in the solution of the laminar Navier-Stokes equations, although they can be suppressed by using the turbulence model. Numerical and experimental factors that are responsible for the deviation of the laminar solutions from experimental results are discussed. The secondary vortex in shock diffraction is successfully simulated by solving the Navier-Stokes equations.

Key words: Secondary vortex, Shock diffraction, Slipstream, Vortex sheet, Shear layer, Numerical methods

1 Introduction

The development of numerical schemes to solve the conservation laws for compressible flows, mainly the Euler equations, has reached a state of maturity. A variety of numerical schemes with high-order accuracy were proposed in the past few decades (Toro, 1999). Most of them provide reasonably good results on both structured and unstructured meshes, and have been extended to other more complicated physical systems. Flows in shock tubes are characterized by their unsteadiness due to the limited test time. It was found that numerical solutions of the unsteady Euler equations reproduce precisely shock propagation, reflections from walls and interaction with bodies. For instance, in shock wave focusing in a large chamber, the difference between experimental photos and numerical solutions of the Euler equations can be within the uncertainty in conventional shock-tube measurements (Sun and Takayama 1996). However, the difference may become distinguishable in some vortical flows, such as shock wave/boundary layer interaction and flows very near a sharp corner. In these cases, viscosity is no longer negligible. An example, which shows the flow behind a diffracting shock wave, is illustrated in Fig. 1.

Correspondence to: M. Sun
(e-mail: sun@ceres.ifs.tohoku.ac.jp)

Shock diffraction, one of the most basic phenomena in shock dynamics, has been often adopted as a numerical test for the simulation of unsteady compressible flows. A benchmark test of shock diffraction over a 90° corner was organized during the 18th International Symposium on Shock Waves; many numerical results and several experimental results were summarized by Takayama and Inoue (1991). By comparing with experimental photos, it is understood that numerical solutions of the Euler equations using high-order Godunov-type schemes, piecewise parabolic method (PPM), finite volume Galerkin scheme (FVGS), FEM-FCT, TVD-type schemes or other schemes can reproduce very well diffracting shock waves, expansion waves and the shape of the main vortex. However, numerical schemes (say, TVD-type and Godunov-type schemes) solved on a reasonably fine grid are found to give thicker contact surfaces, but thinner shear layers. From Fig. 1, other two differences between experiment and numerical solutions are observable. One is that a secondary vortex, which lies below the slipstream and between the corner and the main vortex in experiment, does not show up in numerical solutions of the Euler equations on both coarse and fine grids. Another is, the smooth slipstream shown in the experimental photo develops many small vortices in the numerical solution of the fine grid, as shown in Fig. 1c indicated by arrows.

The formation of the secondary vortex is due to the separation of the boundary layer on the downstream wall; its mechanism was interpreted by Rott (1956). It is expected that if viscosity and heat conductivity are considered numerical calculation should reproduce the secondary vortex, although this has not been reported in open literature to our knowledge. On the other hand, the interpretation for the appearance of small vortices in a numerical simulation is more complicated. On an extremely fine grid, which is usually realized by using the adaptive mesh technique, a thin shear layer can evolve to many small vortices. Uchiyama and Inoue (1995) reported the formation and evolution of these vortices by solving the Euler equations using the flux-vector splitting scheme. Similar phenomena were also observed in the simulation of the Mach reflection over a wedge that contains a slipstream, e.g. Figs. 21, 22, 25, 26 in the benchmark test (Takayama and Jiang 1997), and Fig. 7.1 shown by Berger and Colella (1989). The phenomenon seems to be expected since it is argued that the shear layer is unstable and the Kelvin-Helmholtz instability develops and eventually grows up into small vortices. However, the rolling-up of these small vortices had not been observed in experiments of Skews (1967). Thereafter numerous shock-tube experiments have been conducted in order to observe the phenomenon in our Center using holographic interferometry (e.g. Sun and Takayama 2003); unfortunately, no interferogram convincingly shows the existence of the rolling-up of the small vortices. A typical experimental photo is shown in Fig. 1a, where the slipstream appears to be clearly smooth and continuous.

In numerical simulation, the rolling-up of small vortices is observed on fine grids. Two numerical results, obtained on coarse and fine grid respectively, are given in Fig. 1b and c. The rolling-up of small vortices is not observable in the numerical solution obtained on a coarse grid (Fig. 1b). Comparing two numerical results with the experimental one, one may see that the spiral vortex on the coarse grid is surprisingly closer to experiment.

The motivation of this note is two-fold. One is to verify whether the Navier-Stokes equations can reproduce the secondary vortex observed in experiment, and whether tiny vortices in the Eulerian solutions can be suppressed by adding viscosity and heat conductivity. This note reports the results of this study.

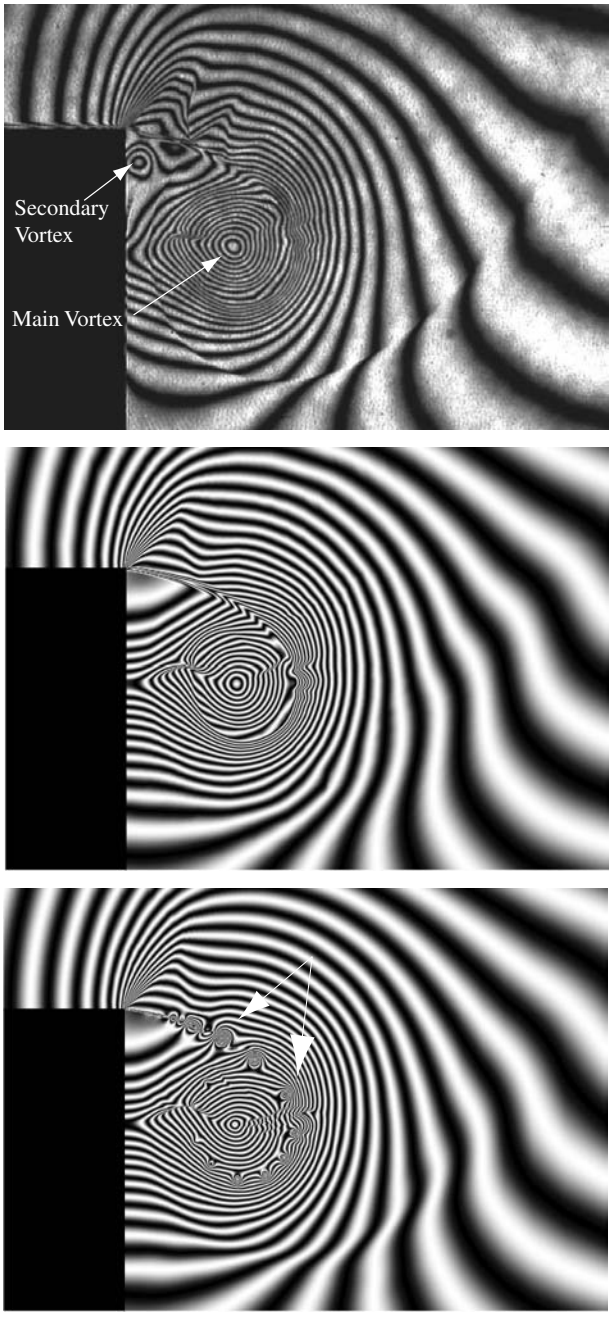

Fig. 1a–c. Vortical structure in shock diffraction, $M_s = 1.5$, **a** is an experimental photo and **b,c** are numerical solutions of the Euler equations; the fringes are contours of the same density: **a** $t = 295$ μs, image size = 104 mm × 73 mm; **b** coarse grid, 300×210; **c** fine grid, 900×630

2 Numerical method

For weak shock waves at room temperature and pressure, any test gas can be considered as perfect gas following the equation of state

$$p = \rho RT, \tag{1}$$

where R is the universal gas constant divided by the molecular weight of the gas. The perfect-gas law is accurate to ±10% in the range $1.8 \leq T/T_{crit} \leq 15$ (White 1974), where T_{crit} is the temperature at the critical point. For air, such a temperature range corresponds to 240 K ∼ 2000 K. As a direct consequence of the perfect-gas law the internal energy becomes, for the constant ratio of specific heats γ,

$$\rho e = \frac{p}{\gamma - 1}. \tag{2}$$

For air, the value of γ is 1.4. All these assumptions are valid for the gas in the present experiment.

The Euler and the laminar Navier-Stokes equations, and the Reynolds average Navier-Stokes equations with the standard $k-\epsilon$ model proposed by Launder and Spalding (1972) coupled with the equation of state (1) and inter-

nal energy (2) are numerically solved by the finite volume method on an all-quadrilateral grid. The method solves them by directly applying them to each quadrilateral cell. The change of conservative quantities in the quadrilateral cell is equal to the summation of fluxes through four interfaces. The Euler solver contains two schemes, centered and upwind schemes, to calculate the fluxes. Both schemes are second-order accurate in time and space. The centered scheme is based on the predictor-corrector Lax-Wendroff scheme, and a non-linear artificial viscosity is added to suppress possible oscillations (Sun 1998, Sun and Takayama 1999). The upwind scheme is the MUSCL-Hancock scheme (see, Toro 1999). The minmod limiter is used to flatten slopes of primitive variables, and the fluxes through interfaces are determined by solving the HLLC approximate Riemann problem.

The governing equations with viscous and heat-transfer terms are solved following the operator-splitting method, $U^{n+1} = NCU^n$, where operator C represents the convection step that solves exactly the equations with convective terms, and operator N represents the viscous step that integrates all other terms. If the convection step and the viscous step are second-order accurate for their own parts, the combination is also second-order accurate. The reader should refer to papers (Strang 1968, Demkowicz et al. 1990) for details. The convection step is solved using the method discussed in the preceding paragraph. The viscous step integrates viscous and heat-transfer terms using the forward-time-central-space (FTCS) scheme. The scheme is second order accurate in space and first order accurate in time. For high Reynolds number flows, the coefficients of the Navier-Stokes specific terms have the order of Δx^2 if one chooses $\Delta x = O(1/\sqrt{R_e})$. That is to say, in most regions, the viscous effects are trivial. For the regions close to solid boundaries, the flow is almost steady. Therefore, the real truncation errors created due to the first-order accuracy in time should not be larger than those introduced in the convection step by a second-order scheme. This greatly simplifies the formulations for solving the viscous terms. The wall surface is assumed to be isothermal. The viscous solver has been validated by testing the Couette flow and the boundary layer over a flat wall.

To be able to efficiently distribute fine meshes around the corner and the wall surface, a solution-adaptive unstructured quadrilateral mesh (Sun and Takayama 1999) is used. The solver uses an initial unstructured quadrilateral mesh that covers a 720 mm long and 120 mm high computational domain, the corner portion of which is shown in Fig. 2a. For the present simple domain, the mesh contains only rectangles. In order to resolve well the boundary layer in viscous computations, the initial mesh cells are clustered to the wall surface, and the cells along the surface are forced to be refined during computation. In the region where the vortical structure form, square cells are used to avoid possible numerical errors due to grid irregularity. An example of solution-adaptive mesh is shown in Fig. 2b, in which important flow features are captured by fine cells such as shock wave, vortex and slipstream, and the fine cells are removed when these features have passed away. A four-level refinement is used in the present computations, and the finest cell size is 0.03 mm in length and height. Although stretched cells are often used in the viscous computation, it is not suitable for the present case because the shear layer lies in the flow field and its orientation is unknown beforehand; so square cells are used to cover the region where vortex forms and the boundary layer separates.

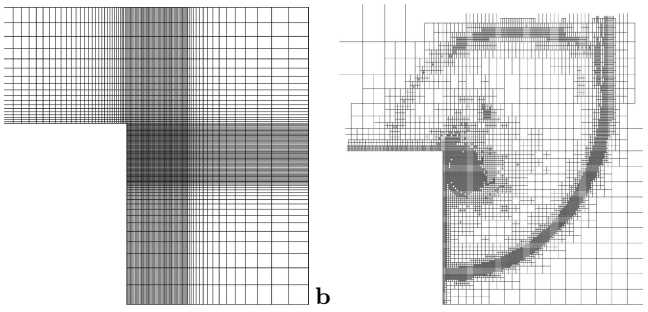

Fig. 2a,b. Numerical mesh: **a** initial mesh, only 1/11 of total length and 1/2 of total height of the whole computational domain is shown; **b** an adaptive mesh, only about 1/13 of mesh **a** is shown, finest cell size = 0.03 mm

3 Results and discussion

Experiments were conducted using a 60 mm × 150 mm diaphragmless shock tube (Yang 1995) in the Shock Wave Research Center, Tohoku University. The flow was visualized by double exposure holographic interferometry using a Q-switched ruby laser with 25 ns pulse duration. The height of shock tube was 150 mm, and the light path 60 mm. Initial pressure in front of shock wave was 92 kPa for shock Mach number $M_s = 1.50$. Test gas was air at 298±2 K during all experiments. The fringes correspond to equal density contours, and the density difference between two fringes is 4.8% of the density in front of the incident shock wave. Numerical simulations were conducted under the same initial conditions.

Figures 1b and c are the Eulerian solutions obtained by the present computation. It is seen that the coarse grid resolves the slipstream in a good agreement with the experiment, while the fine grid produces a few small vortices that are not observed in the experiment, Fig. 1a. Since other researchers have also reported the formation and evolution process of these small vortices in solving the Euler equations, we shall not repeat commenting this aspect here. However, we stress that numerical solutions also indicate that the time in the Eulerian solutions when the small vortices start to appear, t_v, is nearly proportional to the grid size, Δx,

$$t_v = \alpha \Delta x,$$

where α depends on the numerical scheme used. If the velocity is normalized by $(RT)^{1/2}$, coefficient α is about

700 for the MUSCL-Hancock scheme, and 1000 for the centered scheme in our computation. These values agree fairly well with the value 950 for a TVD scheme, which is estimated from the results of Uchiyama and Inoue (1995). It should be noted that t_v, which is a function of grid size, has no physical meaning, mainly because shock diffraction has no length and time scales if viscosity and heat-conductivity are neglected. The finer the grid is, the earlier the small vortices start to appear. Artificial viscosity built in the numerical schemes should play an important role in determining the coefficient α.

The density distributions at different time instants obtained by solving the laminar Navier-Stokes equations are plotted in Figs. 3 and 4. The minimum mesh size is 30 μm, and it is equivalent to 4000×4000 cells for a 120 mm $\times$ 120 mm domain, which is the best resolution we may achieve with a limited computer resource. Even though the mesh Reynolds number is about 200 for a representative velocity of 100 m/s, so the viscous terms are actually under-resolved and physical dissipation on fine vortices may be under-estimated. Note that although flow features in all plots seem to have the same scale, they are actually growing with time. Because the flow features are almost self-similar, spatial coordinates at different instants t are scaled to the same size by dividing the factor t, and their physical scales are given in the captions.

Figure 3 shows the early stage of vortex formation. The slipstream is resolved smoothly. Boundary layers develop on the upstream and the downstream walls, which are not seen in the Eulerian solutions. Although the main flow moves downward, the flow over the downstream wall close to the corner moves upward. The boundary layer there experiences an adverse pressure gradient and separates from the wall, resulting in a secondary vortex, which lies between the main vortex and the corner. The vortex structure resolved in Fig. 3c agrees well with the interferogram in Fig. 1a. However, the numerical time scale is about ten times shorter. The interferogram corresponds to 295 μs after the arrival of shock at the corner, while the numerical result corresponds to 30 μs. Figure 4 shows the numerical results at later time. The slipstream is no longer smooth, and a few small vortices have already formed at $t = 60$ μs as shown in Fig. 4a. These small vortices grow and disturb the flow field significantly. Bifurcated shock waves are visible due to the interaction with the vortices in Fig. 4c. Comparing the small vortices in the laminar solutions with those in the Euler equations, we found that the evolution process is actually very similar, except that the small vortices are slightly attenuated in the Navier-Stokes solution. Figure 4 indicates that viscous dissipation in the laminar Navier-Stokes equations is not sufficient to damp the small vortices. It maybe suggested that the 2-D laminar Navier-Stokes equations still underestimate the physical dissipation of the experiment.

The rolling-up of the two-dimensional small vortices is related to the Kelvin-Helmholtz instability that produces spanwise vortices. In experiment, the flow is three-dimensional. The slipstream is also unstable in another direction and can produce streamwise vorticity, which is certainly not resolvable in 2-D computation. However, it is not possible yet to directly simulate the 3-D Navier-Stokes equations under the present computational resources. A $k - \epsilon$ turbulence model is chosen to investigate whether the small vortices can be suppressed by the turbulent dissipation.

Figure 5 shows the comparison of results of the laminar Navier-Stokes equations and the turbulent model with the experiment at $t = 195$ μs after shock arrival at the corner. The convection terms in both governing equations are solved by the same limiter, approximate Riemann solver, and MUSCL-Hancock scheme, so that the difference between the two numerical results should result from the additional turbulence dissipation in the turbulent model. Numerical simulations with the turbulent model show that small vortices are gradually damped by increasing initial turbulence intensity. The result shown here was obtained for an initial turbulence kinetic energy of $0.036a_0^2$, where a_0 is the sound speed in front of the incident shock wave. Compared with the experiment photo Fig. 5a, the numerical result with the turbulence model reproduces well not only the vortex spiral, the secondary vortex but also the secondary shock structure over the slipstream. By comparing the vortex spiral in Fig. 5b and Fig. 1b obtained by two different governing equations respectively, it can be concluded that artificial viscosity that is built in the numerical scheme solving the Euler equations on a coarse grid may have a similar effect on the shear layer as the turbulence dissipation. Certainly, numerical dissipation cannot replace the physical dissipation in all aspects; for example, it fails to resolve the secondary vortex.

Figure 6 records the trajectories of the vortex core using the three governing equations. Experiments indicated that the trajectory is a straight line (Skews 1967, Yang 1995). The vortex core is numerically located at the cell that has the minimum value of pressure. It is seen that the trajectories given by the Euler equations and the laminar Navier-Stokes equations periodically deviate from the straight line with an increasing amplitude, while the trajectory given by the turbulence model is nearly a straight line. From the viewpoint of vortex dynamics, the small discrete vortices in the solutions of the Euler and the Navier-Stokes equations induce a different velocity at the vortex core from that of a smooth shear layer although their total strength, in terms of circulation, are nearly the same. This further suggests the small vortices in the numerical solutions are not so pronouncing in reality.

4 Remarks on the appearance of small vortices

Slipstreams or vortex sheets are produced from a sharp corner behind a diffracting shock wave or a triple point in Mach reflection. For a shock wave of $M_s = 1.5$ diffracting over a 90° corner, the slipstream, the convective Mach number of which is about 0.7 estimated from an analytical model (Sun and Takayama 2003), is unstable according

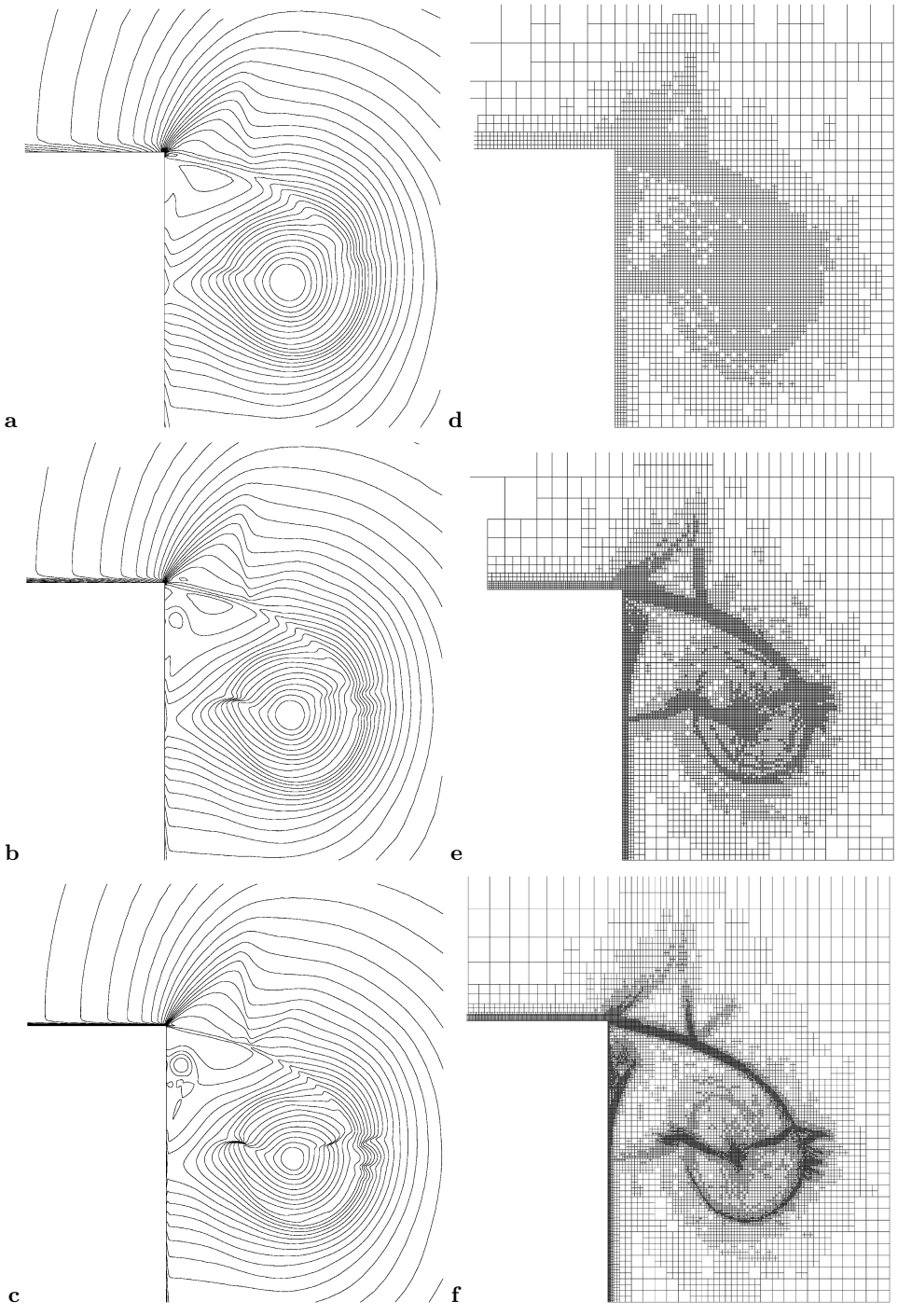

Fig. 3a–f. Numerical solutions of the laminar Navier-Stokes equations (Part 1, smooth shear layer): **a** $t = 10$ μs, 2.16 mm × 2.16 mm; **b** $t = 20$ μs, 4.32 mm × 4.32 mm ; **c** $t = 40$ μs, 8.64 mm × 8.64 mm; **d,e** and **f** correspond to adaptive meshes for **a,b** and **c**, respectively

to the linear stability analysis of Miles (1958) for inviscid flows. Any derivation from the perfect slipstream due to numerical random errors, such as truncation and grid-dependent errors, may trigger the instability. However, if the appearance of small vortices is a consequence of the instable slipstream, it is hard to interpret the fact that the vortices cannot be seen in experiment. Present numerical tests further show that simply considering the effect of viscosity and heat conductivity by using the laminar Navier-Stokes equations cannot suppress these vortices. Two factors, on both experimental and numerical side, are considered responsible for the discrepancy.

In experiment, the optical methods used up to now recorded only the integrated density information across

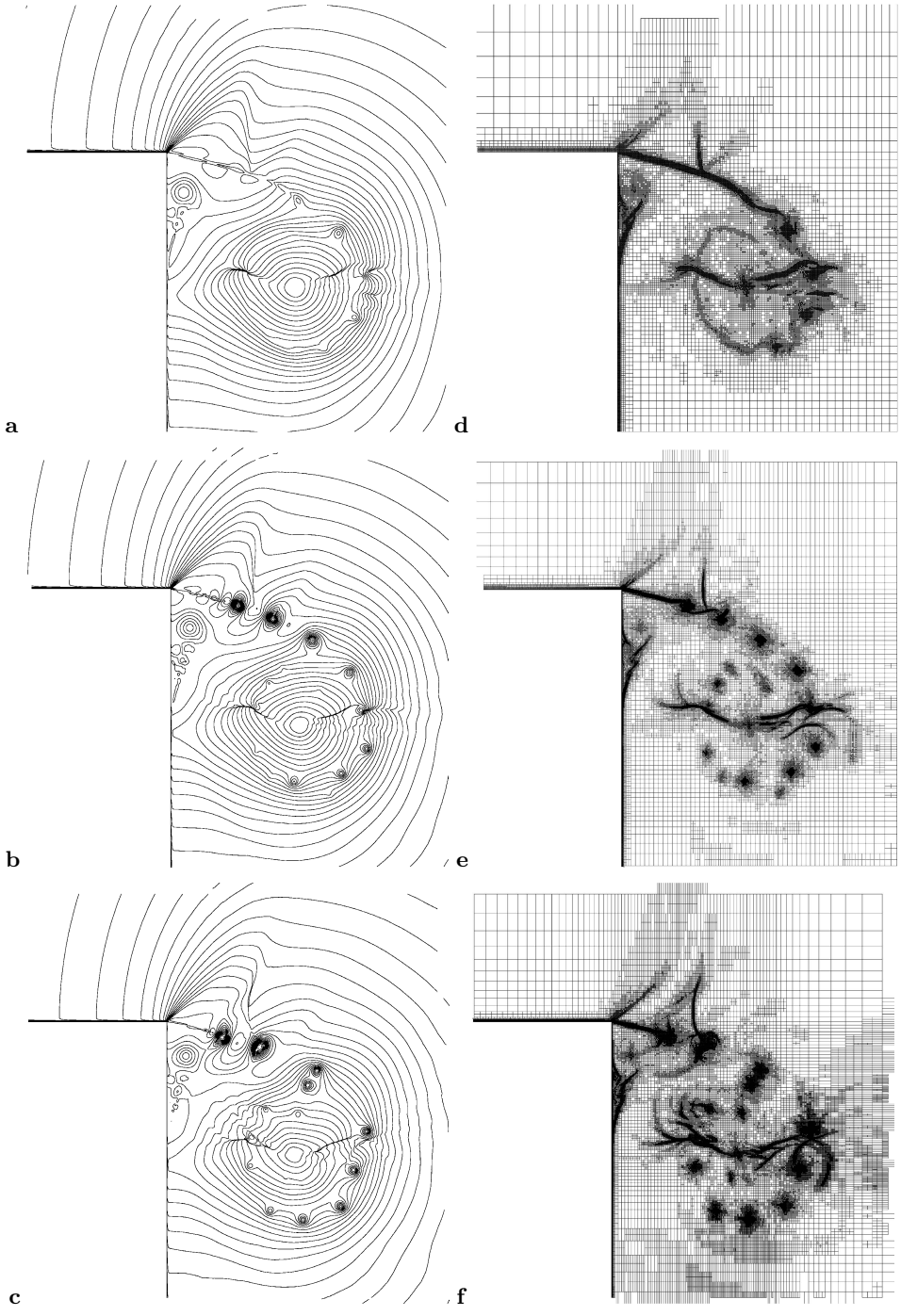

Fig. 4a–f. Numerical solutions of the laminar Navier-Stokes equations (Part 2, small vortices): **a** $t = 60$ μs, 12.96 mm×12.96 mm; **b** $t = 100$ μs, 21.6 mm × 21.6 mm; **c** $t = 140$ μs, 30.24 mm × 30.24 mm; **d,e** and **f** correspond to adaptive meshes for **a,b** and **c**, respectively

the test section. There is a possibility that small vortices may contain three-dimensional perturbations, and so not show up on integrated images. Note that for a viscous flow over a backward-facing step, the flow is often turbulent (e.g. Le et al. 1997). The smooth slipstream obtained by solving the turbulence model somehow supports this interpretation, since the turbulent flows may result from the instable three-dimensional perturbations. Nevertheless, the small vortices in the numerical simulations grow so large as shown in Fig. 5c that it should have been detected by optical methods. The two-dimensional Euler and Navier-Stokes equations exaggerate their evolution, or three-dimensional effects are not the only factor that contributes to the discrepancy.

In the numerical simulation of the Navier-Stokes equation, the flow is under-resolved since the cell Reynolds

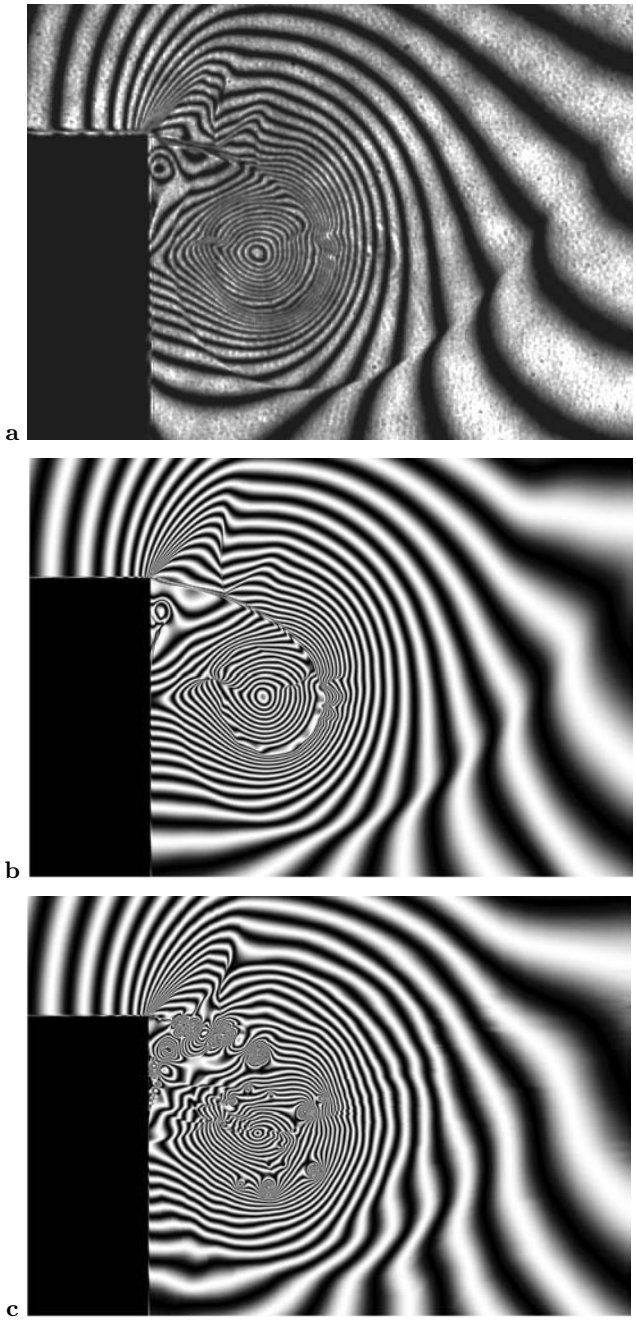

Fig. 5a–c. Comparison of laminar and turbulent solutions with experiment, $M_s = 1.5$, $t = 195$ μs, image size = 70 mm × 49 mm; the fringes are equal density contours: **a** experimental photo; **b** solution of the $k-\epsilon$ turbulence model, mesh size 2300 × 1600; **c** solution of the 2-D laminar Navier-Stokes equations, mesh size 2300 × 1600

number is rather high. It has been reported that under-resolved solutions contain spurious nonphysical vortices (Brown and Minion 1995) in incompressible flow simulations of a vortex sheet. Although the numerical mechanisms responsible for the artifacts have not been clearly understood, the spurious vortices share a few similarities as the small vortices observed in simulation of shock diffraction, such as both central and upwind schemes can

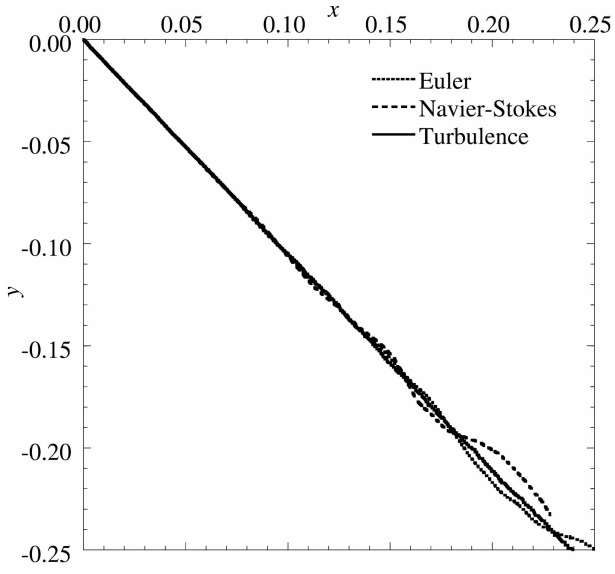

Fig. 6. Trajectories of the main vortex core

produce such artifacts. Those spurious vortices may result in the small vortices in compressible simulation of a shear layer, or at least disturb the evolution of the shear layer. Note that the under-resolved problem cannot be avoided by using a fine grid. The grid size is limited by available computer resources; more importantly for the Euler equations, numerical solutions are always under-resolved whatever the grid size is if the Euler equations are considered as the Navier-Stokes equations with an infinitely large Reynolds number. Another interesting numerical experiment done by Samtaney & Pullin (1996) suggests a grid-converged smooth numerical solution of the vortex sheet exists, by solving the self-similar solution of the compressible equations, or a boundary value problem. Then the problem left is how to construct a numerical method that does not or weakly disturb the smooth solution. Existing numerical methodology seems not up to this problem.

5 Concluding remarks

Numerical solutions of the Navier-Stokes equations confirm that the secondary vortex in shock diffraction is due to the viscous effect. We successfully reproduce by numerical simulation both the complete vortex system and the fine wave structure near the corner in shock diffraction. This, to our knowledge, is reported for the first time in the literature.

The rolling-up of small vortices along a vortex sheet, which was reported in solving the Euler equations but never been observed in shock tube experiment, appears also in the solution of the 2-D Navier-Stokes equations, but may be suppressed by using a turbulence model. The numerical mechanism of the rolling-up in numerical simulation is still a controversial issue. Existing numerical methods behave badly in solving such a problem. Some novel numerical methods are required to suppress or attenuate the small vortices without degrading the accuracy

in other regions. This would pose a considerable challenge for computational fluid mechanics.

References

Berger MJ, Colella P (1989) Local adaptive mesh refinement for shock hydrodynamics. J. Comput. Phys. 82: 64

Brown DL, Minion ML (1995) Performance of under-resolved two-dimensional incompressible flow simulations. J. Comput. Phys. 122: 165

Demkowicz L, Oden JT, Rachowicz (1990) A new finite element method for solving compressible Navier-Stokes equations based on an operator splitting method and $h-p$ adaptivity. Comput. Methods Appl. Mech. Engrg. 84: 275

Launder BE, Spalding DB (1972) Mathematical models of turbulence. Academic Press, New York, London

Le H, Moin P, Kim J (1997) Direct numerical simulation of turbulent flow over a backward-facing step. J. Fluid Mech. 330: 349

Miles JW (1958) On the disturbed motion of a plane vortex sheet. J. Fluid Mech. 3: 538

Rott N (1956) Diffraction of a weak shock with vortex generation. J. Fluid Mech. 1: 111

Samtaney R, Pullin DI (1996) On initial-value and self-similar solutions of the compressible Euler equations. Phys Fluids 8: 2650

Skews BW, (1967) The perturbed region behind a diffracting shock wave. J. Fluid Mech. 29: 705

Strang G, (1968) On the construction and comparison of difference schemes. SIAM J. Numer. Anal. 5: 506

Sun M, Takayama K (1996) A holographic interferometric study of shock wave focusing in a circular reflector. Shock Waves 6: 323

Sun M, (1998) Numerical and experimental studies of shock wave interaction with bodies. Ph.D. thesis, Tohoku University, Japan, http://ceres.ifs.tohoku.ac.jp/~sun/thesis.html

Sun M, Takayama K (1999) Conservative smoothing on an adaptive quadrilateral grid. J. Comp. Phys. 150: 143

Sun M, Takayama K (2003) Vorticity production in shock diffraction. J. Fluid Mech. 478: 237

Takayama K, Inoue O (1991) Shock wave diffraction over a 90 degree sharp corner, Posters presented at 18th ISSW. Shock Waves 1: 301

Takayama K, Jiang Z (1997) Shock wave reflection over wedges: a benchmark test for CFD and experiments. Shock Waves 7: 191

Toro EF (1999) Riemann solvers and numerical methods for fluid dynamics. 2nd edition, Springer. Berlin, Heidelberg, New York

Uchiyama N, Inoue O (1995) Adaptive mesh refinement computation of compressible flows. Shock Waves @ Marseille I, edited by Brun R and Dumitrescu LZ, pp. 407–412, Springer, Berlin, Heidelberg, New York

White FM (1974) Viscous fluid flow. McGraw-Hill, Inc, New York

Yang JM (1995) Experimental and theoretical study of weak shock wave. Ph.D. Thesis, Tohoku University, Japan